A Novel Vectorial Unified Transform for the Full-Wave Broadband Characterization of On-chip Passives

Tim Pattyn[1], Daniël De Zutter[1], Martijn Huynen[1] and Dries Vande Ginste[1]
[1]*quest, Department of Information Technology, Ghent University - imec, Belgium*

***Abstract*—We present a novel framework for deriving the three-dimensional (3-D) differential surface admittance (DSA) operator. The approach is based on a new unified transform method for the 3-D vector Helmholtz equation. This formulation enables a broader applicability than existing DSA derivation techniques, without compromising its accuracy. The effectiveness of the proposed method is verified through a representative scattering problem, and its practical utility is further demonstrated by evaluating the impedance response of an on-chip stacked spiral inductor.**

***Index Terms*—3-D differential surface admittance (DSA) operator, single-source boundary integral equation (BIE), vectorial unified transform, on-chip inductor**

I. Introduction

THE demand for higher processing speeds and greater integration density continues to grow across the electronics industry. These trends aggravate signal integrity (SI) issues which can be detrimental for the performance of modern electronic systems. In particular, passive components exhibit markedly different behavior at high frequencies, for example due to self-resonances or (unintended) coupling between adjacent circuit sections. Accurate full-wave modeling of all components during the early design stages is therefore essential. However, attaining accurate full-wave results efficiently is often non-trivial. While volumetric methods typically result in an impractically large number of unknowns, boundary-based methods face challenges associated with the precise numerical integration of the Green's function in conductive media [1]. The differential surface admittance (DSA) operator has previously been proposed as a solution to this limitation [2] and successfully applied to the modeling of 3-D on-chip passives [3]. It enables replacing the object's material with the background medium by introducing a fictitious surface current density on its surface, thereby eliminating dependence on the Green's function within the object's interior region.

In this work, we introduce a new method for constructing the 3-D DSA operator, by formulating a novel vectorial unified transform [4]. In contrast to state-of-the-art DSA-based techniques, the proposed method eliminates the need for the object's eigenmodes [5] or material-specific Green's functions [6] in the operator's derivation. Consequently, the resulting formulation offers a broader scope of applicability while retaining all favorable properties of the DSA framework.

This work was supported by the Research Foundation-Flanders (FWO) under Grant 1S04425N.

II. Formulation of the Method

Consider time-harmonic electromagnetic fields $(\mathbf{e}_{\text{inc}}, \mathbf{h}_{\text{inc}})$, with an $e^{j\omega t}$ dependence, incident on a cuboid composed of an isotropic, non-magnetic and homogeneous material with complex wavenumber k_i. The cuboidal domain is denoted by $\mathcal{V}$, with surface $\mathcal{S}$, outward-pointing normal vector $\mathbf{u}_n$, and embedded in a surrounding medium characterized by its wavenumber $k_e \in \mathbb{C}$, as illustrated in Fig. 1a. The excitation results in scattered fields in the exterior region $(\mathbf{e}_{\text{sc}}, \mathbf{h}_{\text{sc}})$ and interior fields within the cuboid $(\mathbf{e}_i, \mathbf{h}_i)$. By invoking the single-source equivalence theorem, the object's material is replaced by the background medium through the introduction of a fictitious surface current density $\mathbf{j}_s$ on the boundary $\mathcal{S}$ while preserving the field distribution on the outside. The surface current density is given by:

$$\mathbf{j}_s = \hat{\mathbf{n}} \times (\mathbf{h}_i - \mathbf{h}_i') = (\mathcal{P} - \mathcal{P}_0)\mathbf{e}_0^t \triangleq \mathcal{Y}\mathbf{e}_0^t, \qquad (1)$$

where $\mathbf{e}_0^t$ denotes the total tangential electric field on $\mathcal{S}$ and $\mathcal{Y}$ is the corresponding DSA operator. The latter can be interpreted as the difference between the Dirichlet-to-Neumann (DtN) operators $\mathcal{P}$ and $\mathcal{P}_0$, which map the tangential electric field on $\mathcal{S}$ to the rotated tangential magnetic field for the original and equivalent situations shown in Fig. 1, respectively.

In order to solve the boundary value problems needed to obtain the DtN operators, we propose a new *vectorial* unified transform for the vector Helmholtz equation. We refer the interested reader to [7] for a detailed explanation on the scalar 3-D unified transform. Fundamentally, the unified transform relies on a global relation, which connects the known and unknown boundary values. In

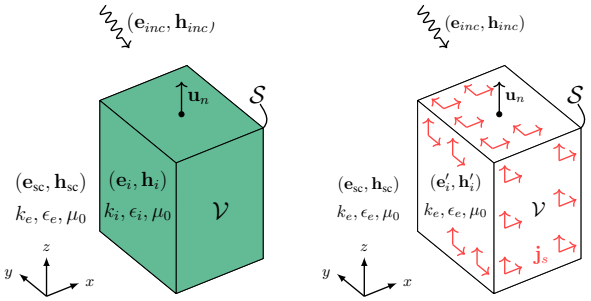

Fig. 1: Geometry of the problem: (a) Homogeneous cuboid $\mathcal{V}$ with boundary surface $\mathcal{S}$ placed inside a background medium. In (b), a surface current $\mathbf{j}_s$ is introduced on $\mathcal{S}$ and the inner material is replaced by the background medium.

our proposed method, this role is fulfilled by the electromagnetic reciprocity theorem:

$$\iint_{\mathcal{S}} (\mathbf{e}_i \cdot \hat{\mathbf{h}}_t - \mathbf{e}_t \cdot \hat{\mathbf{h}}_i) dS = 0, \tag{2}$$

where we introduced the scaled and rotated tangential magnetic field $\hat{\mathbf{h}}_i = Z_c(\mathbf{u}_n \times \mathbf{h}_i)$ and similarly for $\hat{\mathbf{h}}_t$. The characteristic impedance Z_c of the medium filling the cuboid is defined as $Z_c = \sqrt{\frac{\mu_0}{\epsilon_i}}$, and $\mathbf{e}_t$ and $\hat{\mathbf{h}}_t$ are — as yet — arbitrary test fields, constrained solely by the requirement that they satisfy the sourceless Maxwell's equations within $\mathcal{V}$.

In the following, we only consider the bottom face of the cuboid as the so-called observer face $\mathcal{S}_o$ oriented in the xy-plane with dimensions $\{l_x, l_y\}$, but the derivation is readily extended to the other faces of the cuboid. Legendre polynomial–based basis functions are employed to exploit their orthogonality on $\mathcal{S}_o$:

$$f_{nm}(x, y) = P_n\left(\frac{x}{l_x/2}\right) P_m\left(\frac{y}{l_y/2}\right), \tag{3}$$

where $P_n(x)$ is the Legendre polynomial of order n and argument x. On $\mathcal{S}_o$, the tangential field components of the unknown solution $(\mathbf{e}_i^o, \hat{\mathbf{h}}_i^o)$ are expanded using these Legendre basis functions with $e_{nm}^{o,x}$ the expansion coefficient for the x-oriented tangential electric field on face o related to the basis function $f_{nm}(x, y)$ and a similar definition holds for $\hat{h}_{n'm'}^{o,x}$. Inserting these expansions into the l.h.s. of (2) yields:

$$\begin{aligned}\sum_{n,m} \iint_{\mathcal{S}_o} ((e_{nm}^{o,x}\ \mathbf{u}_x + e_{nm}^{o,y}\mathbf{u}_y) \cdot \hat{\mathbf{h}}_t) \\ \times f_{nm}(x - x_o, y - y_o) dS \\ - \sum_{n',m'} \iint_{\mathcal{S}_o} (\mathbf{e}_t \cdot (\hat{h}_{n'm'}^{o,x}\mathbf{u}_x + \hat{h}_{n'm'}^{o,y}\mathbf{u}_y)) \\ \times f_{n'm'}(x - x_o, y - y_o) dS. \end{aligned} \tag{4}$$

The unified transform exploits the fact that, when a sufficiently rich set of test solutions $(\mathbf{e}_t, \hat{\mathbf{h}}_t)$ is employed, the resulting overdetermined system yields an accurate approximation of the DtN operator. For these test solutions, we use 2×6 sets of plane waves, i.e., a pair of sets originates from each face of the cuboid. For example, the relevant field expressions for the test plane waves originating from the source face $\mathcal{S}_s$, oriented in the yz-plane with a negative outward-pointing normal vector, i.e., the leftmost face of the cuboid, are provided below:

$$\text{set 1:} \quad \mathbf{e}_t^1 = \mathbf{p}_1 e^{-j\phi},\ \hat{\mathbf{h}}_t^1 = (\mathbf{u} \times \mathbf{p}_1) e^{-j\phi}, \tag{5}$$

$$\text{set 2:} \quad \mathbf{e}_t^2 = \mathbf{p}_2 e^{-j\phi},\ \hat{\mathbf{h}}_t^2 = (\mathbf{u} \times \mathbf{p}_2) e^{-j\phi}, \tag{6}$$

with

$$\mathbf{u} = \frac{k_y \mathbf{u}_y + k_z \mathbf{u}_z + k_x \mathbf{u}_x}{k}, \quad \tau = \sqrt{k_y^2 + k_z^2}, \tag{7}$$

$$\mathbf{p}_1 = \frac{k_z \mathbf{u}_y - k_y \mathbf{u}_z}{\tau}, \quad \mathbf{p}_2 = \mathbf{u} \times \mathbf{p}_1 \tag{8}$$

$$\phi = k_x(x - x_s) + k_y(y - y_s) + k_z(z - z_s), \tag{9}$$

$$k_y = \frac{M\pi}{\beta l_y}, \quad M = -M_{max}, \ldots, M_{max}, \quad M \in \mathbb{Z}, \tag{10}$$

$$k_z = \frac{P\pi}{\gamma l_z}, \quad P = -P_{max}, \ldots, P_{max}, \quad P \in \mathbb{Z}, \tag{11}$$

$$k_x = \sqrt{k_i^2 - k_y^2 - k_z^2}, \tag{12}$$

where (x_s, y_s, z_s) are the coordinates of the centroid of the source plane $\mathcal{S}_s$. The two sets of test fields are defined as plane waves propagating along $\mathbf{u}$. In the yz-plane, the real wavenumbers k_y and k_z enable a Fourier-type sampling, while the parameters β and γ regulate the sampling density. The square root for k_x should be picked such that $\Re(k_x) \geq 0$ and $\Im(k_x) \leq 0$. The specific choices for k_x, k_y, and k_z ensure that the resulting electric fields have unit amplitude on $\mathcal{S}_s$, with amplitudes that remain constant or decay as the waves propagate in the positive x-direction. This prevents exponential growth of the test waves inside the cuboid, which is essential for numerical stability. The two sets of test waves, (5) and (6), are orthogonal, enabling explicit incorporation of polarization within the unified transform formalism. The expressions for the test solutions (5)-(12)

also extend naturally to other faces of the domain with different orientations.

Evaluating (5) on $\mathcal{S}_o$, inserting the result into the global relation (4) and computing all scalar and vector products as well, results in:

$$\sum_{n,m}\left(\frac{k_x k_y}{k\tau}e^{o,x}_{nm}+\frac{\tau}{k}e^{o,y}_{nm}\right)A^{so}_{nm}-\sum_{n',m'}\frac{k_z}{\tau}\hat{h}^{o,y}_{n'm'}A^{so}_{n'm'}, \tag{13}$$

with

$$A^{so}_{nm}=l_x l_y(-j)^{n+m}j_n\left(\frac{k_x l_x}{2}\right)j_m\left(\frac{k_y l_y}{2}\right)\times e^{j(k_x x_s+k_y y_s+k_z(z_s-z_o))}. \tag{14}$$

In (14), $j_n(x)$ represents the spherical Bessel function of order n and argument x. Following a similar procedure for the second set of test plane waves (6) yields:

$$\sum_{n,m}\frac{-k_z}{\tau}e^{o,x}_{nm}A^{so}_{nm}- \sum_{n',m'}\left(\frac{-\tau}{k}\hat{h}^{o,x}_{n'm'}+\frac{k_x k_y}{k\tau}\hat{h}^{o,y}_{n'm'}\right)A^{so}_{n'm'}. \tag{15}$$

Although not explicitly shown, (13) and (15) each correspond to $(2M_{\text{max}}+1)(2P_{\text{max}}+1)$ equations, resulting from the sampling of the test waves. A similar procedure is performed for all pairs of faces of the cuboid. Collecting the Legendre expansion coefficients for the tangential electric field on all the faces, e.g., $e^{o,x}_{nm}$ and $e^{o,y}_{nm}$, in the column vector $\bar{\mathbf{e}}$ and the Legendre coefficients for the scaled, rotated tangential magnetic field, e.g., $\hat{h}^{o,x}_{nm}$ and $\hat{h}^{o,y}_{nm}$, in the column vector $\bar{\hat{\mathbf{h}}}$, allows to write these $6\times 2\times(2M_{max}+1)(2P_{max}+1)$ equations as a single analytically constructed matrix equation:

$$\bar{\bar{D}}\cdot\bar{\mathbf{e}}-\bar{\bar{N}}\cdot\bar{\hat{\mathbf{h}}}=0. \tag{16}$$

To obtain a square system, we premultiply (16) by the conjugate transpose of $\bar{\bar{N}}$, resulting in:

$$\bar{\mathbf{h}}=\frac{1}{Z_c}(\bar{\bar{N}}^H\bar{\bar{N}})^{-1}\bar{\bar{N}}^H\bar{\bar{D}}\cdot\bar{\mathbf{e}}=\bar{\bar{\mathcal{P}}}\cdot\bar{\mathbf{e}}, \tag{17}$$

where $\bar{\bar{\mathcal{P}}}$ denotes the desired discretized DtN operator for the cuboid $\mathcal{V}$. Using the aforementioned method, we determine the two DtN operators $\bar{\bar{\mathcal{P}}}$ and $\bar{\bar{\mathcal{P}}}_0$ constituting the discretized DSA operator $\bar{\bar{\mathcal{Y}}}$:

$$\bar{\mathbf{j}}_s=(\bar{\bar{\mathcal{P}}}-\bar{\bar{\mathcal{P}}}_0)\cdot\bar{\mathbf{e}}\triangleq\bar{\bar{\mathcal{Y}}}\cdot\bar{\mathbf{e}}, \tag{18}$$

By following a procedure closely related to the one outlined in [5], we project (18) onto rooftop functions, allowing seamless integration with traditional boundary integral equation (BIE) formulations such as the augmented electric field integral equation [8]. The result is a linear system that provides full, broadband characterization of the electromagnetic problem.

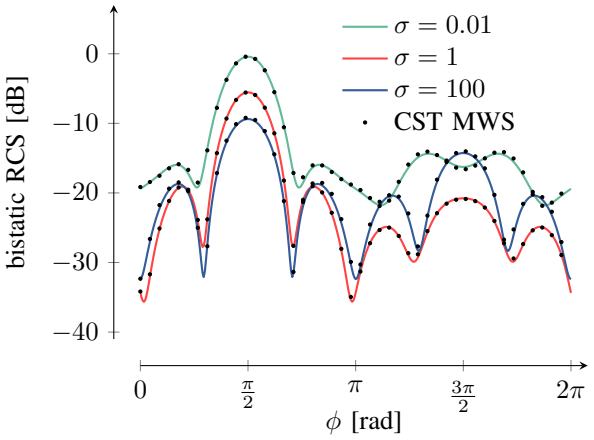

Fig. 2: Bistatic RCS in the xy-plane of a cuboid with $\epsilon_r = 3.9$ and varying electrical conductivity σ. The plane wave is propagating in the positive y-direction with a z-polarized electric field at a frequency of 2 GHz.

III. Numerical Examples

To validate the accuracy of our proposed approach, we first consider a cuboid with dimensions $20\text{ cm}\times 12\text{ cm}\times 6\text{ cm}$ that consists of a material with fixed relative dielectric constant $\epsilon_r = 3.9$ and varying conductivity σ. The surface of the cuboid is discretized using 1404 rooftop functions, while the DSA operator is constructed by employing 450 Legendre basis functions and 1922 test waves per face with a sampling density of 0.8. A plane wave traveling in the positive y-direction with a z-polarized electric field at a frequency of 2 GHz is incident on the cuboid. The resulting bistatic radar cross-section in the xy-plane as a function of the azimuth angle ϕ is provided in Fig. 2 for three distinct values of σ. We compare our new method with the results obtained from CST Microwave Studio's (CST MWS) frequency-domain solver [9], a commercial finite-element based solver. An excellent agreement is observed between both solutions for all values of σ, highlighting the accuracy of our proposed formalism for a wide range of material parameters. Moreover, on average across all three values of σ, our proposed method is a factor 5.6 faster compared to CST MWS while using 4.3 times less memory, underscoring its efficiency in addition to its accuracy.

For the second example, we focus on the stacked spiral on-chip inductor structure, depicted in Fig. 3. The three inductor windings are made of copper ($\sigma = 5.8\times 10^7$ S/m) and are embedded in an SiO_2 background medium ($\epsilon_r = 3.9, \tan\delta = 0.001$). The windings have a width of 5 µm and a height of 2 µm. The vias connecting the different windings have a cross-section

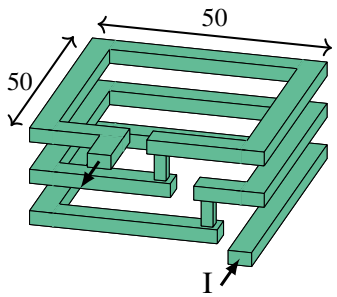

Fig. 3: On-chip stacked inductor structure consisting of copper windings ($\sigma = 5.8 \times 10^7$) and embedded in a SiO_2 background ($\epsilon_r = 3.9, \tan\delta = 0.001$).

of 2.5 µm × 2.5 µm and a height of 4 µm. The other relevant dimensions are indicated on Fig. 3 and are expressed in µm.

As for the validation example, the results shown in Fig. 4 and obtained with the proposed method are compared against CST MWS. In the inductive operation region, i.e., from 0.5 GHz to 50 GHz, the proposed method exhibits excellent agreement with the CST MWS reference solution, yielding a simulated inductance L = 0.487 nH. As the frequency increases into the (first) self-resonant region, between 50 GHz and 150 GHz, where the inductor's inductance and parasitic capacitance interact, the correspondence between both solutions remains strong. At lower frequencies, from 0.01 GHz to 0.5 GHz, the results diverge: the proposed method correctly predicts the impedance approaching the DC resistance R = 0.91 Ω, whereas CST MWS fails to capture this behavior accurately. The DC resistance was obtained from a static volumetric solver. This limitation underscores the appositeness of our presented approach, which provides reliable impedance characterization across the entire frequency range, unlike the commercial tool.

IV. Conclusions

This contribution introduced a novel framework for deriving the 3-D differential surface admittance operator. The approach is based on the construction of a new vectorial unified transform to solve the 3-D vector Helmholtz equation. Therefore, it employs the electromagnetic reciprocity theorem as the global relation in conjunction with plane-wave testing and Legendre polynomial basis functions. The validity of the approach was confirmed through comparison with a commercial solver, and its practical relevance was demonstrated via the analysis of an on-chip stacked spiral inductor. The proposed method accurately captured the inductor's impedance response across the full frequency range, whereas the commercial tool failed to cover the entire frequency band.

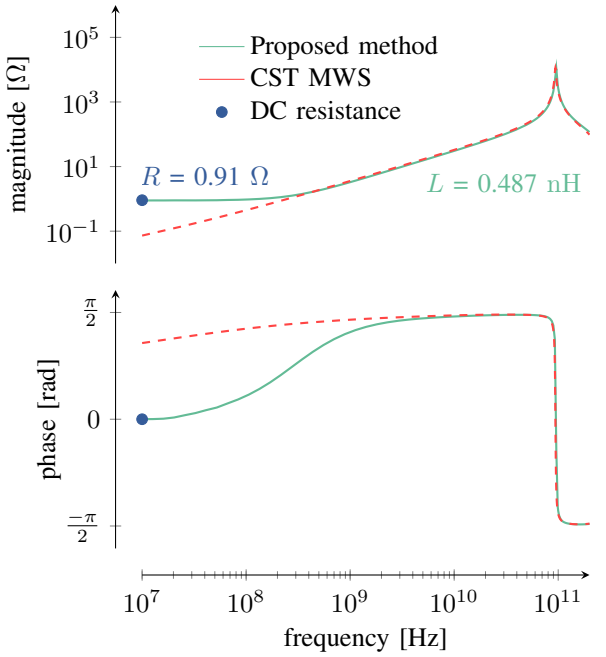

Fig. 4: Magnitude (top) and phase (bottom) of the impedance response from the on-chip inductor presented in Fig. 3.

References

[1] J. Peeters, I. Bogaert, and D. De Zutter, "Calculation of MoM interaction integrals in highly conductive media," *IEEE Transactions on Antennas and Propagation*, vol. 60, no. 2, pp. 930–940, 2012.

[2] D. De Zutter and L. Knockaert, "Skin effect modeling based on a differential surface admittance operator," *IEEE Transactions on Microwave Theory and Techniques*, vol. 53, no. 8, pp. 2526–2538, 2005.

[3] T. Pattyn, X. Sun, E. Beyne, D. De Zutter, M. Huynen, and D. Vande Ginste, "Broadband electromagnetic modeling of on-chip passives using a differential surface admittance operator for 3-D piecewise homogeneous structures," *IEEE Transactions on Microwave Theory and Techniques*, vol. 73, no. 12, pp. 10199–10212, 2025.

[4] A. S. Fokas, *A Unified Approach to Boundary Value Problems*. Society for Industrial and Applied Mathematics, 2008.

[5] M. Huynen, K. Y. Kapusuz, X. Sun, G. Van der Plas, E. Beyne, D. De Zutter, and D. Vande Ginste, "Entire domain basis function expansion of the differential surface admittance for efficient broadband characterization of lossy interconnects," *IEEE Transactions on Microwaves Theory and Techniques*, vol. 68, no. 4, pp. 1217–1233, 2020.

[6] U. R. Patel, S. Sharma, S. Yang, S. V. Hum, and P. Triverio, "Full-wave electromagnetic characterization of 3D interconnects using a surface integral formulation," in *Proc. IEEE 26th Conf. Elect. Perform. Electron. Packag. Syst.*, pp. 1–3, oct. 2017.

[7] A. C. L. Ashton, "Elliptic PDEs with constant coefficients on convex polyhedra via the unified method," *Journal of Mathematical Analysis and Applications*, vol. 425, no. 1, pp. 160–177, 2015.

[8] Z.-G. Qian and W. C. Chew, "Fast full-wave surface integral equation solver for multiscale structure modeling," *IEEE Transactions on Antennas and Propagation*, vol. 57, no. 11, pp. 3594–3601, 2009.

[9] Dassault Systèmes, *CST Studio Suite*, 2024. https://www.3ds.com/products-services/simulia/products/cst-studio-suite.